Influence of double-stage operation on breathing oscillations and rotating spokes in the ID-HALL thruster

IEPC-2019-632

Presented at the 36th International Electric Propulsion Conference
University of Vienna • Vienna, Austria
September 15-20, 2019

A. Guglielmi[1] A. Martín Ortega[2], F. Gaboriau[3] and J.P. Boeuf [4]
LAPLACE, Université de Toulouse, CNRS, INPT, UPS, 118 Route de Narbonne, 31062 Toulouse, France

and

C. Boniface[5]
Centre National d'Etudes Spatiales (CNES), 18 avenue Edouard Belin, 31401, Toulouse, France

Abstract: ID-HALL is a double stage Hall thruster where the ionization stage is a magnetized radiofrequency (RF) inductively coupled plasma located upstream and close to the acceleration stage. In this paper we show that operation in a double-stage mode can significantly affect electron transport and instabilities in the magnetized plasma of ID-HALL. Large amplitude low frequency oscillations (breathing mode), present in a single-stage regime of operation, are strongly damped when the RF power in the ionization stage is turned on. Time-resolved RPA measurements show that the plasma potential in the ionization source is modulated in time when operating in a breathing mode due to a modulation of the plasma conductivity in the anode region. Time-resolved CCD images of the light emitted by the thruster show that rotating spokes present in the thruster channel in a single-stage regime of oscillations tend to disappear when operating in a double-stage mode while plasma rotation at lower velocities is observed in the ionization chamber.

I.Introduction

A new concept of Double-Stage Hall Thruster (DSHT), called ID-HALL for **I**nductively **D**ouble stage **Hall** thruster (patent pending), is being developed and tested at the LAPLACE laboratory in Toulouse. The characteristic feature of ID-Hall is that the ionization stage is a magnetized inductively coupled plasma source where the RF coil is placed inside the central cylinder of the thruster. As discussed in previous papers[1-3], the design of ID-Hall is such that the ionization source is as close to the magnetic barrier as possible. Magnetic cusps are arranged in the ionization stage to enhance the RF power coupling and to limit charged particle losses to the walls. In this paper we use time-resolved diagnostics (time-resolved Retarding Potential Analyzer - RPA, and CCD imaging) to study breathing oscillations and plasma rotation in single-stage and double-stage regimes of operation of ID-Hall. The experimental set-up and diagnostic techniques are described in section II. Time-resolved RPA measurements of the Ion Energy Distribution Function (IEDF) are presented in section III, and results of CCD imaging of rotating plasma structures are discussed in section IV.

[1] PhD Student, Univ. Toulouse, guglielmi@laplace.univ-tlse.fr
[2] Research engineer, IRT Saint Exupéry, martin-ortega@laplace.univ-tlse.fr
[3] Associate Professor, Univ. Toulouse, freddy.gaboriau@laplace.univ-tlse.fr
[4] Directeur de Recherche (Senior Scientist) CNRS, jpb@laplace.univ-tlse.fr
[5] Electric propulsion R&T manager, CNES, French Space Agency, claude.boniface@cnes.fr

II. Experimental set-up and diagnostics

In this section we briefly present the ID-Hall prototype used in the experiments and describe the principles of the time resolved RPA and CCD imaging diagnostics.

A. Experimental set-up

Figure 1 shows a schematic and a 3D view of the studied ID-Hall prototype. For this prototype the coil is 25 mm long and 20 mm in diameter, with 11 turns around a ceramic support. A low-loss ferrite of 10 mm diameter is placed in the center of the coil to act as a magnetic conductor for both the DC field creating the magnetic barrier and the RF field of the inductive source. Two ferrite discs of 22 mm diameter are placed on both extremities of the inductive coil, with 1mm thick samarium-cobalt (SmCo) magnets placed around the ferrite discs. The magnetization inside the magnetic barrier near the exhaust plane is directed in the radial direction from the outer to the inner channel (looking at the thruster from the exhaust side, the $E \times B$ drift is therefore clockwise oriented in the azimuthal direction). The assembly of the inductive coil, ferrite and magnets is contained inside a 26-mm diameter Quartz tube which also acts as the insulating inner wall of the thruster.

The outer wall is made of alumina and has two distinct regions: a cylindrical channel of 46 mm diameter and 10 mm length and a conical-shaped wall that extends from the channel diameter to a 92 mm diameter in a length of 30 mm. Two sets of SmCo magnets are placed in the back of the ionization chamber in the conical wall and in the inner cylinder. Both sets of magnets are kept in place by an L-shaped soft iron piece; this piece also closes the DC magnetic circuit. The magnets and magnetic circuit create 4 magnetic cusps with magnetic field lines parallel to the walls in the ionization chamber, reducing the ion losses at the walls and increasing the plasma density. In addition to the magnetic barrier in the channel near the exhaust plane, a second magnetic barrier is created at the base of the ionization chamber in front of the anode. The use of ferrite material inside the coil (instead of soft iron in our first design of ID-Hall[2]) tends to decrease the magnetic field along the inner cylinder wall and move the zero magnetic field region closer to the wall. The consequence is a less efficient confinement of the plasma and a larger loss of ions to the inner wall. This will be corrected in future prototypes.

The anode consists of a copper disc of 40 mm diameter and 4 mm width, covered on the back side and on the inner and outer diameters by an insulating ceramic, so that only the front side of the disc is exposed to the plasma. The anode is placed at the maximum of the second magnetic barrier, so that the surface of the disc is approximately parallel to the magnetic field lines. The position can be adjusted axially.

Xenon is injected at the base of the ionization chamber after passing through a disc of porous ceramics (Mullite 250). The cathode used in this study, provided by the ICARE laboratory, is a hollow cathode with a LaB_6 disc placed behind the aperture and heated by a tungsten filament. A starter was used to trigger the discharge but was not required during continuous operation of the thruster. The RF power source was an RFG 50-600 from Coaxial Power Systems operating at 4 MHz. The reduced frequency (with respect to the standard 13.56 MHz) was chosen to reduce the capacitive coupling and the losses in the central ferrite; a side-effect is the increase of the current and the ohmic losses.

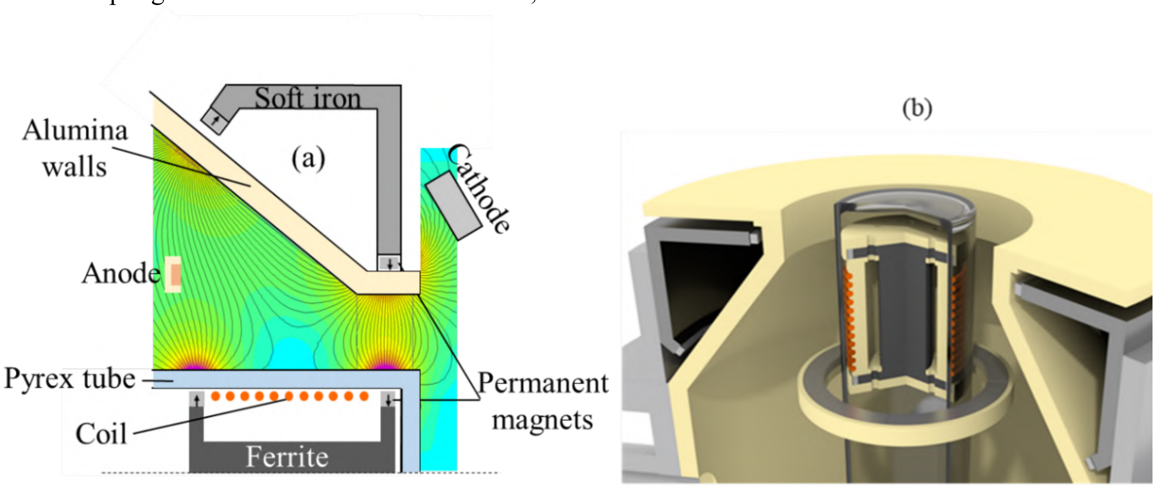

Figure 1. (a) Schematic of the experimental prototype of ID-Hall used in this study, showing the magnetic field lines. (b) 3D view of the thruster channel, RF coil inside the inner cylinder, and ionization stage.

B. Time resolved RPA (Retarding Potential Analyzer) measurements

The RPA used in this study was developed in the group of A. Bouchoule at the GREMI laboratory of the University of Orleans in 1998. Its design and operating conditions are reported in the PhD thesis of C. Philippe-Kadlec[4]. Even though this RPA is mounted on a rotative arm, all measurements presented here are performed at 55 cm in front of the exhaust plane of the thruster. The RPA uses a set of electrostatic grids to selectively repel electrons from the plasma and a collector to measure the current and the Ion Energy Distribution Function (IEDF). Two of these grids are set at -35 V and -40 V to prevent respectively external electrons from entering the RPA and secondary electrons from being emitted away from the collector surface. The voltage of the third grid of the RPA is swept from zero to a high positive voltage to collect ions of different energies. This grid is controlled with a triangular voltage at 500 Hz (this frequency is much lower than the frequency of any oscillation observed on the discharge current). The collector is connected to the oscilloscope through a 1MΩ impedance. A band-reject filter is added to the circuit to reduce the 4 MHz RF noise from the source. For time integrated measurements of the IEDF, the signal is averaged by the oscilloscope over 128 periods to improve the Signal to Noise Ratio. Both analyzing voltage and RPA signal are recorded using a digital oscilloscope. The derivative of the recorded signal with respect to the voltage is calculated using a Stavisky-Golay filter to obtain the IEDF.

We also performed time-resolved RPA measurements of the IEDF to analyze the behavior of the ion beam when low frequency (breathing mode) oscillations in the 10-30 kHz range were present. Oscillations of the discharge current were used as a time reference to achieve various temporal acquisitions of the current collected by the RPA by gradually varying the voltage of the repulsive grid. In this way, only ions with an energy higher than the voltage applied on the grid are collected by the RPA. For each voltage (with a 5V step), the current characteristics of the RPA collector are obtained as a function of time. The IEDFs are then deduced from the I-V characteristic at each time t. Once the time evolution of the IEDF is obtained at the RPA location, one can deduce the IEDF at the thruster exhaust plane. This can be done by calculating the time of flight of the ions over the distance D_{RPA} from the exhaust plane to the RPA (55cm). This time depends on the ion speed $v_{E_c} = \sqrt{2E_c/M_i}$ where E_c is the measured ion kinetic energy and M_i the ion mass. For each point of IEDFs, the time scale t' at exhaust is deduced from the time t at the RPA location by $t' = t - D_{RPA}/v_{E_c}$.

C. High speed camera imaging of plasma rotation

In Hall thrusters, electrons are strongly magnetized while ions are not. The large azimuthal $E \times B$ and $\nabla P \times B$ electron drifts can induce charge separation and instabilities. The presence of azimuthal plasma non-uniformities ("rotating spokes") in single stage Hall thrusters has been reported by a number of authors[5-10]. Because of a more complex magnetic field configuration, the ID-Hall thruster is a good candidate for the development of rotating structures both in the acceleration stage and in the ionization stage.

In order to characterize these rotating structures, we used a FASTCAM MiniAX50/100 camera with 16-bit grayscale data coding, a 105 mm lens diameter with a 62 mm focal length. This camera can capture speeds of more than 500000 fps (frame per second). However, the capture speed is constrained by the size of the window to be recorded. The larger the image size, the more pixels it will contain and the slower the capture speed and vice versa. To meet our needs, we chose a window of 128x64 pixels and a maximum capture speed of 127500 fps for these dimensions. This capture speed allows us to observe structures moving at a maximum speed of 7.500 km/s. Beyond this speed and with our thruster dimension, the spokes go more than half a turn between two images and it is no longer possible to differentiate a spoke with a high rotational speed rotating clockwise from a slower spoke rotating in counter clockwise (Shannon's sampling limit).

Because of the double stage design and the geometry of the thruster with a classical accelerator channel and a large ionization chamber upstream, we wanted to locate these azimuthal instabilities in 3D along the r, θ and z axes. Previous high-speed camera investigations of azimuthal instabilities in single-stage thrusters were performed without axial resolution. One way to get information both on the azimuthal and axial positions of the spokes is to take images from two points of view sufficiently distant from each other, as shown in Figure 2. The first point of view was fixed in front of the thruster on the axis of the thruster (z axis). The angle at this position is noted $i_{axis} = 0°$. The second point of view was chosen by experimental constraint and to minimize the loss of information in the prolongation of the wall of the chamber at the angle $i_{cam} \simeq 30°$. The images obtained at these two points of view, separated by an incidence of 30° and 3 m from the thruster, must then be recorded simultaneously by the camera. To do this, we positioned a reflective mirror on each of these points of view in order to return images of the thruster on a 90° prism (Figure 2a).

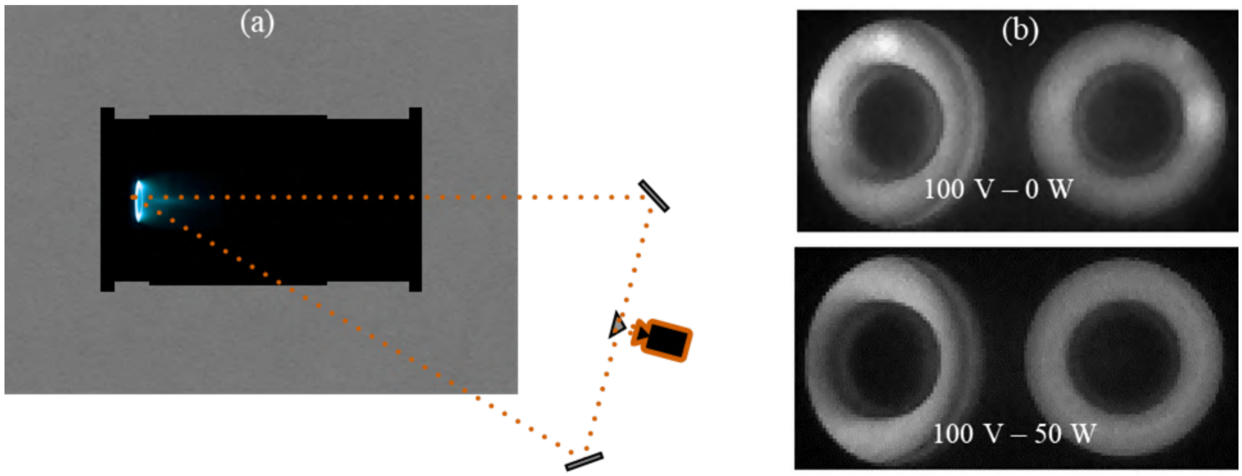

Figure 2. (a) Schematic representation of the experimental device seen from top, showing the chamber, the thruster, the optical elements, the camera and the optical path (dotted lines). (b) Examples of images recorded by the camera under different conditions of voltage and injected RF power in xenon (9 sccm anode mass flow rate).

The two images of the thruster obtained under two different points of view are then recorded simultaneously by the camera as shown in Figure 2b. This optical measurement method has the advantage of being non-intrusive and sensitive enough to locate axially the rotating spokes. The objective is to be able to distinguish the three main regions of the thruster where these structures appear, i.e. in the channel, in the middle of the ionization chamber near the ICP source, and close to the anode. To obtain clear information on the space and time evolution of the plasma non-uniformities, data processing was necessary because of the low signal to noise ratio, of the relatively small number of pixels, and of the conical geometry of the ionization chamber with a smaller channel diameter (Figure 1). In order to determine the parameters of these azimuthal instabilities (speed, mode, size, position $\mathrm{r}, \theta, \mathrm{z}$) from the CCD images, a code was developed under MATLAB® (Matrix Laboratory). This code is split into two main parts, a first part treating the front image and determining the speed and frequency of rotation, angular velocity and mode and a second part using the two points of view and a parallax method to locate image by image the spokes in $(\mathrm{r}, \theta, \mathrm{z})$ and to determine their size.

Data processing program : 1) Speed, frequency and mode of the rotating spokes

We first determine the center and the outlines of the thruster in order to apply a mask revealing only the channel. In addition to deleting data in regions of too low emission, precise application of this mask is necessary for the second 3D part. The program then unfolds, for each image, the light ring formed by the channel by projecting the Cartesian view x, y into an azimuthal view θ, r (non-conformal transformation). We then integrate in r the (θ, r) luminous intensity profile to focus on the θ dependence. These operations are successively applied on 100 to 150 images to obtain a temporal evolution $L_S(\theta, t)$ of the light intensity, as shown in Figure 3a.

The effect of the breathing mode can be eliminated by normalizing the $L_S(\theta)$ curves of each image by their maximum intensity:

$$||L_S(\theta,t)||_L = \frac{L_S(\theta,t)}{\max(L_S(\theta,t))}$$

In order to enhance the visibility of low intensity spokes with respect to brighter spokes we also normalize the luminous intensity in θ, by the temporal average at this angle:

$$||L_S(\theta,t)||_{L,\theta} = \frac{||L_S(\theta,t)||_L}{<||L_S(\theta,t)||_L>_t}.$$

Figure 3 compares the images obtained with and without this treatment.
Note that normalization by the maximum light intensity is an instantaneous treatment of the image while normalization by time averaging at each angle requires a series of images containing azimuthal variations of light and is therefore a global treatment of the image.

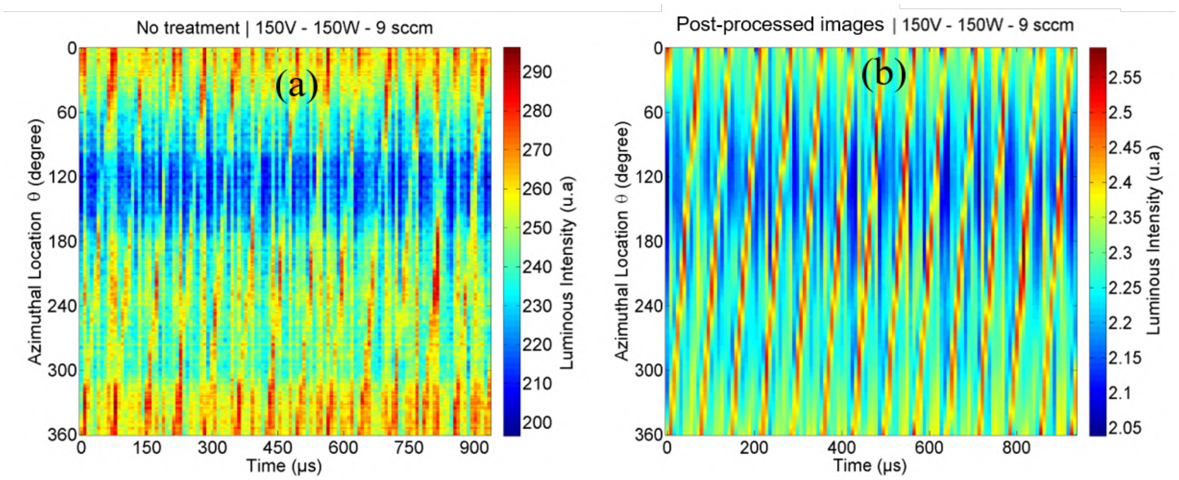

Figure 3. Comparison of (a) the raw images extracted from the thruster channel, (b) with those obtained after image processing, (b). Discharge voltage : 150V - injected RF power : 150W – anode mass flow : 9sccm with stainless steel anode.

After obtaining these images highlighting the azimuthal instabilities over time, it is easier to determine the speed, the rotation frequency and the mode. Different methods have been used in the literature to find the rotation speed of the spokes: manual inspection of the maxima over time [11, 12], Fourier transform of the luminous intensity of the image recorded by the camera, discrete Fourier transform with the use of spoke surface[13] and image segmentation[10]. We used another method based on the properties of the 2D Fourier transforms to determine the rotation speed of the spokes. In the presence of spokes moving with a certain velocity, the results $||L_S(\theta,t)||_{L,\theta}$ are a succession of bands whose inclination is directly connected to the speed of the spokes. The bands will be more vertical as the speed of rotation is larger.

The application of a Fourier transform to an image containing regular bands reveals in the Fourier space fundamental and harmonic frequencies in the direction perpendicular to the bands (Figure 4a). These peaks are therefore directly related to the slope of the lines in real space. Using the positions of each peak in the frequency space, a linear regression of the maxima yields the slope, shown in green in Figure 4a. The latter being strictly perpendicular to the regular bands in real space, the inclination of these bands is therefore equal to $-\frac{1}{a}$; we can then draw on the graph $||L_S(\theta,t)||_{L,\theta}$ of Figure 4b the straight lines of slope $-\frac{1}{a}$.

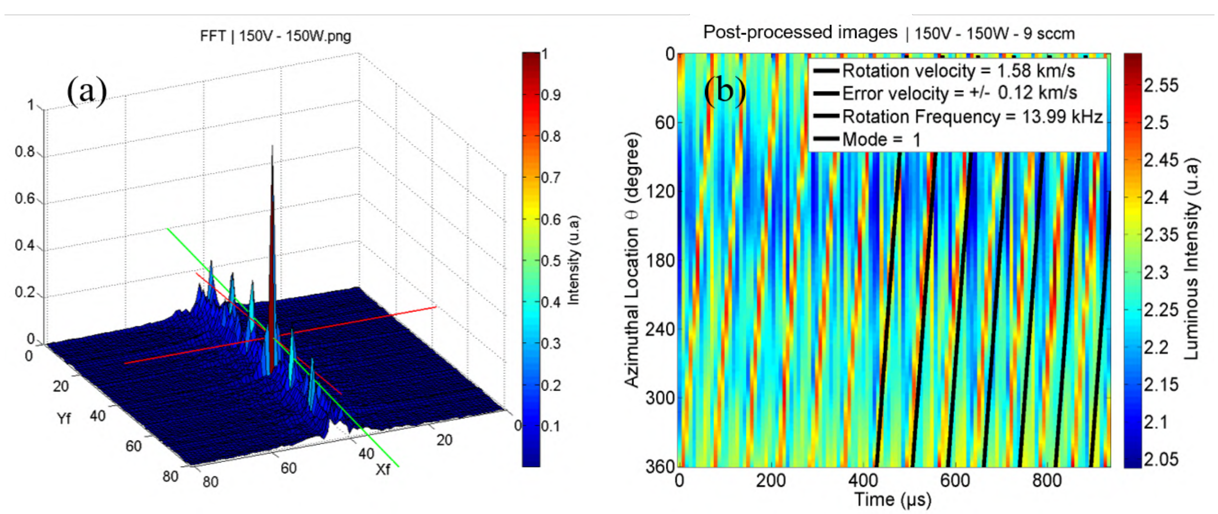

Figure 4. (a) 3D view of the Fourier transform of Figure 3b. The red lines are the main axes, the green line is the one crossing the peaks which characterizes the inclination of the bands in the real image. (b) $||L_S(\theta,t)||_{L,\theta}$ smoothed with, in black, some examples of lines whose slope is derived from the Fourier transform.

The rotation speed v_s and frequency f_s of the spokes are $v_s = |-a|^{-1}\, 2\pi R_m/\Delta t$ and $f_s = v_s/(2\pi R_m)$, with R_m the mean radius of the channel, and Δt the time interval between 2 images (7.8µs). Error speed is determined from the divergence of peaks in the Fourier space.

The number of modes for each case is determined by the ratio between the frequency deduced from the speed of rotation of the spokes and the frequency of oscillation of the luminous intensity for an angle θ as a function of time.

Data processing program: 2), 3D analysis

In the conditions considered here, parallax is a sufficiently sensitive method for determining the axial position of instabilities. Using two different points of view of the same object, it is possible to obtain the position of this object in a plane. We note d_s the distance between the images of a spoke taken by the two cameras in the exhaust plane, as shown in Figure 5. Due to the particular geometry of ID-Hall, there are some shading effects due to the opaque walls of the thruster and spokes that are close to the conical wall cannot be clearly seen. The following assumptions have been made to obtain the different axial positions z_s of the spokes:

- The plasma is considered optically thin: the photons emitted by the plasma are not reabsorbed.
- Optical instabilities are spherical.
- For each path, the two reflecting walls (mirrors and prism) and the transparent elements (glass windows of the box and various optics in the lens of the camera) between the plasma and the camera have negligible geometric aberration and light absorption.
- The optical paths of the two points of view are horizontal and in the same plane.
- Relative to the size of the thruster, the recording of images is at a distance large enough to consider an orthographic projection and therefore without perspective: the vanishing point is located at infinity.
- The range of azimuthal instabilities is bounded laterally by the thruster walls and axially by the anode at the bottom and by the exhaust plane.

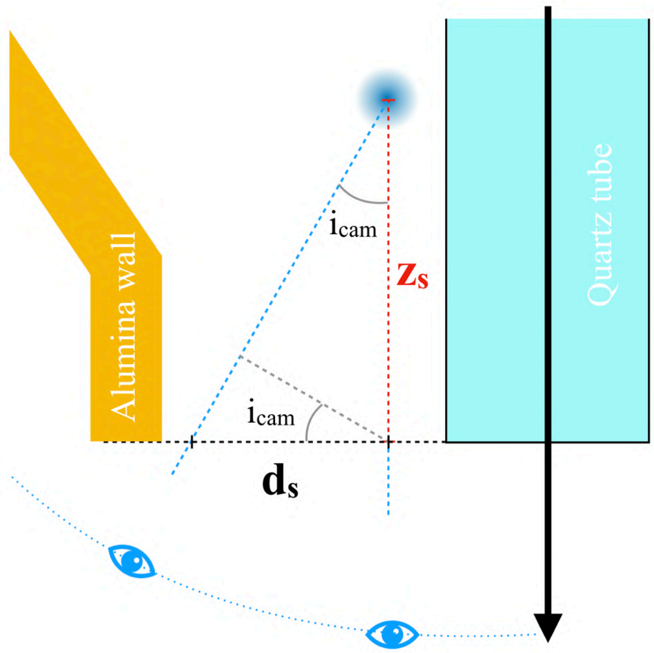

Figure 5. Schematic representation of a (r, z) section of the ID-Hall thruster and the different characteristic lengths to be determined for the parallax method.

From these assumptions, the axial position of the spokes is determined by the distance separating the maxima between two points of view d_s as illustrated in Figure 6. Note that (*i*): for each pixel of each image, the constant brightness was subtracted obtained by averaging over 100 images (the spokes become more marked and the alumina channel on the side view is not visible because the light that it reflects was subtracted) and (*ii*) the side view was stretched in the tilt direction to apply the same circular mask to the front and side views.

From the front view, the positions in r and θ of the spokes indicated by a green dot encircled with black in Figure 6 are determined. On the side view ($i_{cam} = 30°$), the program determines the maximum brightness (blue point encircled in black) on the side of the inclination of the camera (here on the left) and at the same height of each maximum localized on the front face. The distance d_s is then determined for each spoke and the depth z_s from:

$$z_s = \frac{d_s . cos(i_{cam})}{sin(i_{cam})} = \frac{d_s}{tan(i_{cam})}$$

Note that a $cos(i_{cam})$ appears in the equation because the side view has been stretched to apply a circular mask. It is therefore necessary to compensate for this stretch to obtain the actual depth of each spoke.

From the images recorded in perspective and in the (r, z) plane, the program can then reconstruct a 3D view of the spokes (Figure 6c, d).

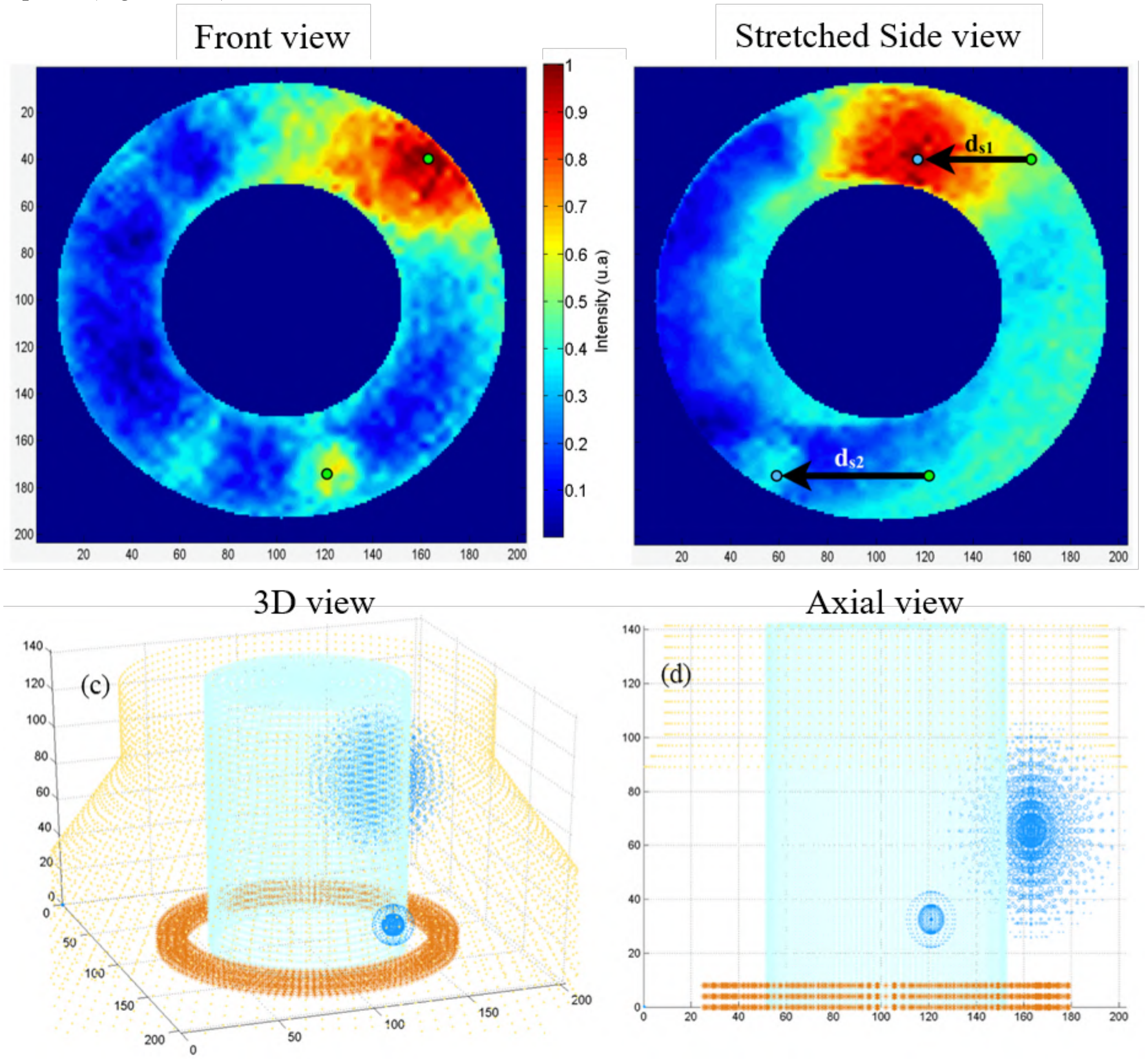

Figure 6. (a) False color representation of the instantaneous luminosity of the plasma seen axially to which the DC component is subtracted and then adjusted to a minimum of zero. The two green dots represent the centers of two local maxima, the two spokes. (b) False color representation of the side view. The blue dots represent the local maxima on the side view with d_{s1} and d_{s2} the distances separating the spokes seen from the front and from the side. (c) – (d) 3D perspective and profile views of the thruster walls (yellow and cyan), anode (orange) and spokes (blue spheres).

III.Breathing mode in single and double stage regimes of operation

The operation of the ID-HALL thruster was first characterized in a single stage mode, with a xenon flow rate of 6 sccm. The corresponding maximum ion current I_{ion} is 0.45A assuming full ionization and single charged ionized ions. The cathode flow rate is 1.5 sccm. The measured I-V characteristics are shown in Figure 7a together with the oscillation amplitude; Figure 7b displays the IEDFs for different discharge voltages.

Depending on the cleanliness of the channel walls, the thruster starts with the help of the cathode keeper, for a voltage between 100V and 250V; the starting voltage is higher for important wall deposit. The current is 0.68 A at 100 V, has a relative maximum of 0.73 A around 120V, and increases again above 200 V (this continuous increase of the current at higher voltages is typical of thrusters with alumina walls[14]).

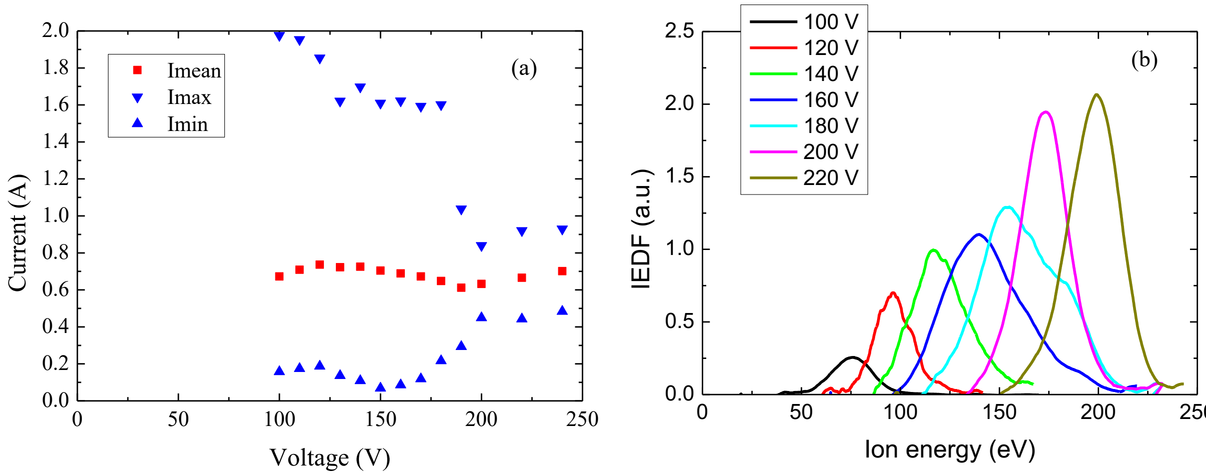

Figure 7. (a) Current-voltage characteristic of the thruster in single-stage (P_{RF}=0 W); (b) IEDF integrated over time for different discharge voltages. The anode mass flow rate is 6 sccm.

Two different operating modes are present below and above a discharge voltage of 190 V in single-stage operation. At low voltages, the discharge current is around 0.7A with a slight decrease as the discharge voltage increases. In this mode of operation, the current has strong regular oscillations of amplitudes 1.5 to 2A (about 3 times the average current). These oscillations from 6 to 15 kHz correspond to oscillations of the "breathing mode". Above 190V, the discharge current monotonically increases with the voltage while the breathing mode disappears.

The time integrated Ion Energy Distribution Function (IEDF) is shown in Figure 7b for different values of the applied voltage. Between 100 and 180 V, the profile of the IEDF is wide and its intensity increases with the applied voltage. The relatively large spread in energy of the IEDF below 190 V is actually due to the presence of two different peaks in energy averaged over time (this can be clearly seen on Figure 7b for a voltage of 180 V).

The time evolution of the IEDF at the exhaust plane in the breathing mode, displayed in Figure 8, shows that the maximum energy of the ions is modulated in time. This temporal IEDF is reconstructed from the RPA measurements as described above in section II.B. The overall maximum of the IEDF occurs for an energy of about 125 eV at t=8 µs on the time scale of Figure 8a but it clearly appears on Figure 8b that this maximum moves back and forth in energy as a function of time. These large variations of the energy at the peak of the IEDF are attributed to time variations of the plasma potential. The possible existence of oscillations of the plasma potential in the breathing mode are confirmed by simulations performed with the HALLIS hybrid model[15] (results not shown here).

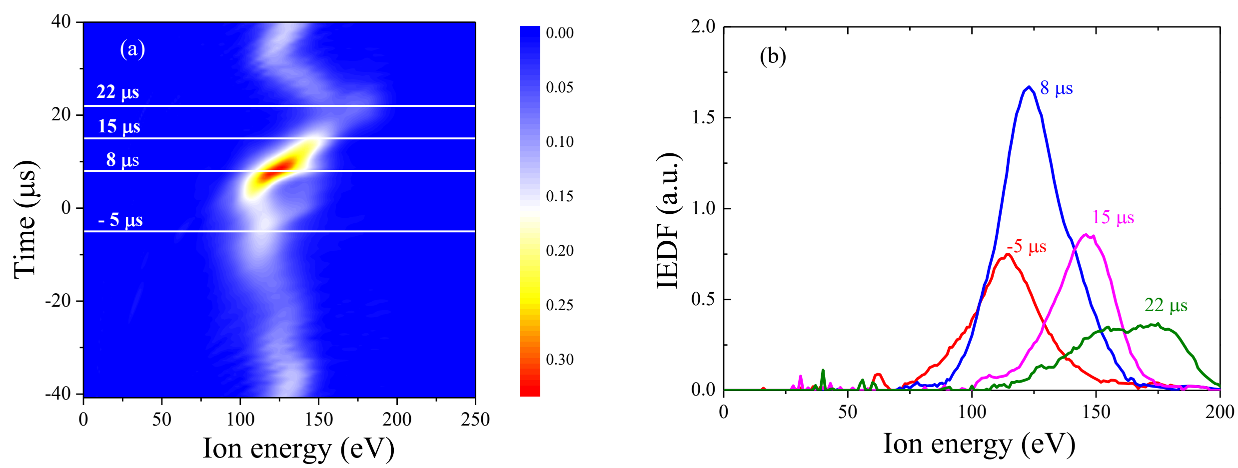

Figure 8. (a) Time evolution of IEDF at the exhaust plane for a 150V discharge voltage (single-stage regime, P_{RF}=0 W); (b) Ion energy distribution at 4 different times corresponding to the white lines of Figure 8a. The anode mass flow rate is 6 sccm.

Previous simulations in a single stage mode of operation with the hybrid HALLIS code and in the absence of breathing mode have shown[2], that a potential drop may exist in the anode region due to the presence of a second magnetic barrier in this region. When breathing oscillations are present, the simulations (not shown here) predict, under some conditions, that the potential drop in the anode magnetic barrier can be modulated in time. Therefore the potential drop on the cathode side, seen by the ions, is also modulated in time, leading to variations with time of the ion energy at the IEDF maximum, as seen in the experimental results of Figure 8. In a double-stage operation of ID-Hall, the plasma density in the ionization stage increases due to power deposition by the RF source and the electron conductivity increases in the ionization chamber and in the anode magnetic barrier. The potential drop in the anode magnetic barrier therefore gradually decreases when the RF power increases, the plasma potential is no longer modulated in time, and the IEDF becomes steady in time, with a narrower distribution in energy.

IV. Instabilities and plasma rotation from ICCD measurements

Regular rotating spokes were observed in ID-Hall at low discharge voltages, below 150V, i.e. under conditions where breathing oscillations were also present (see above). The RF power in the ionization stage has also an influence on the presence of rotating structures, as shown below.

We carried out fast camera measurements as a function of the RF power P_{RF} for 3 different discharge voltages, 0 V, 50 V, and 100 V. The RF power was varied in the range (90W, 150W) at 0 V, (40 W, 150W) at 50 V, and (0 W, 150W) at 100 V. The anode was, as above, located in the second magnetic barrier and the flow rates were respectively 9 sccm at the anode and 1.5 sccm at the cathode. Note that RF power is the injected power and not to the power absorbed by the plasma. ICP source efficiency is presented in the companion paper [16].

Figure 9 shows an example of measured $L_S(\theta, t)$ on a sequence of 150 images for a discharge voltage of 100 V, and for six values of the injected RF power P_{RF}. The discharge voltage is sufficiently large to sustain the plasma in a single stage mode (i.e. for P_{RF} =0 W). It appears in Figure 9a that for the P_{RF} =0 W and P_{RF} =10 W cases, the light intensity at a given θ is modulated in time at the frequency of the breathing oscillations. We can also see on this figure that several instabilities in the azimuthal direction can exist inside each maximum of breathing oscillation. Above P_{RF} =10W, the amplitudes of the discharge current and light intensity oscillations of the breathing mode are quickly damped as can be seen for the P_{RF} =20W and P_{RF} =30W cases of Figure 9b and the P_{RF} =40W and P_{RF} =50W cases on Figure 9c.

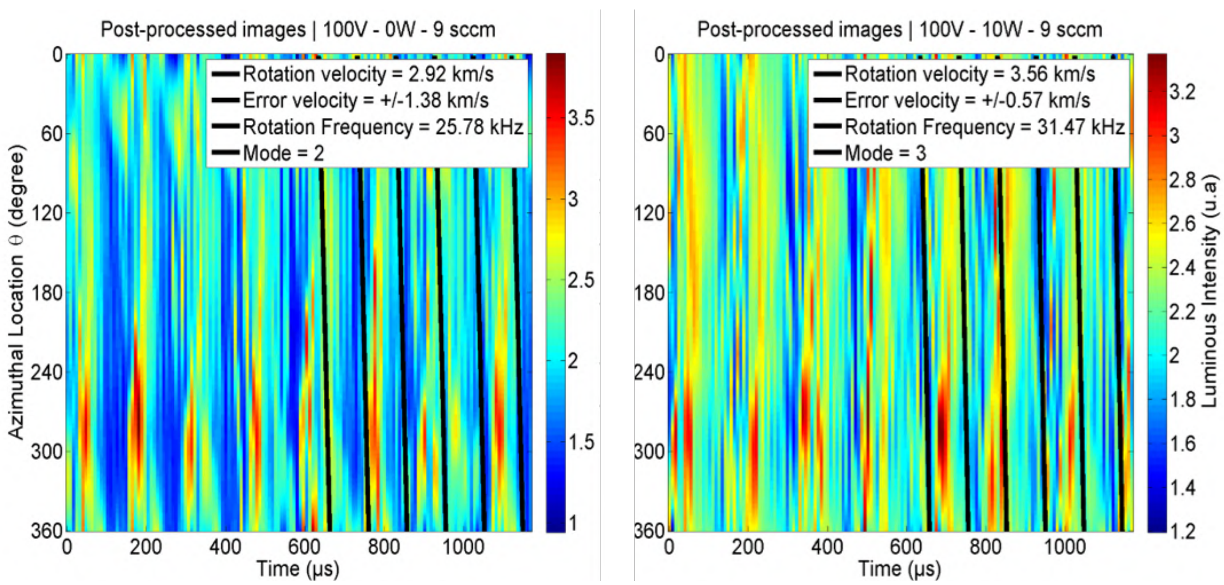

Figure 9. (a) Post-processed images of $L_S(\theta, t)$ for P_{RF} = 0 W and P_{RF} = 10 W of RF power injected. The anode mass flow rate is 9 sccm and the discharge voltage is 100V.

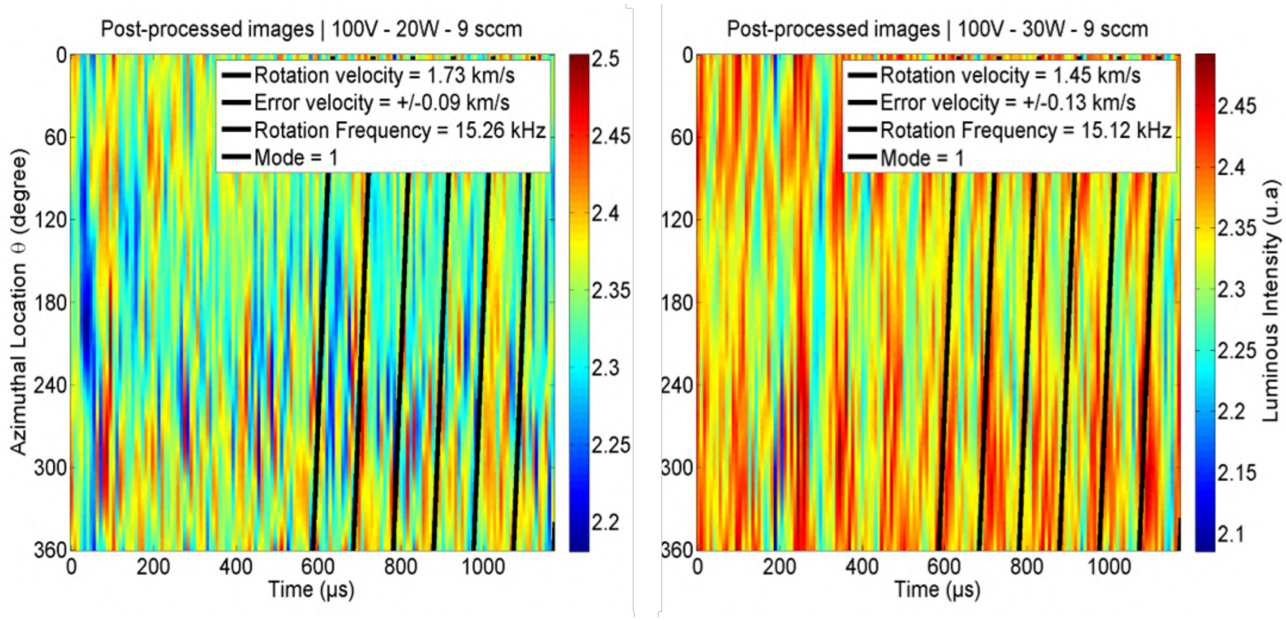

Figure 9. (b) Post-processed images of $L_S(\theta, t)$ for P_{RF} = 20 W and P_{RF} = 30W of RF power injected. The anode mass flow rate is 9 sccm and the discharge voltage is 100V.

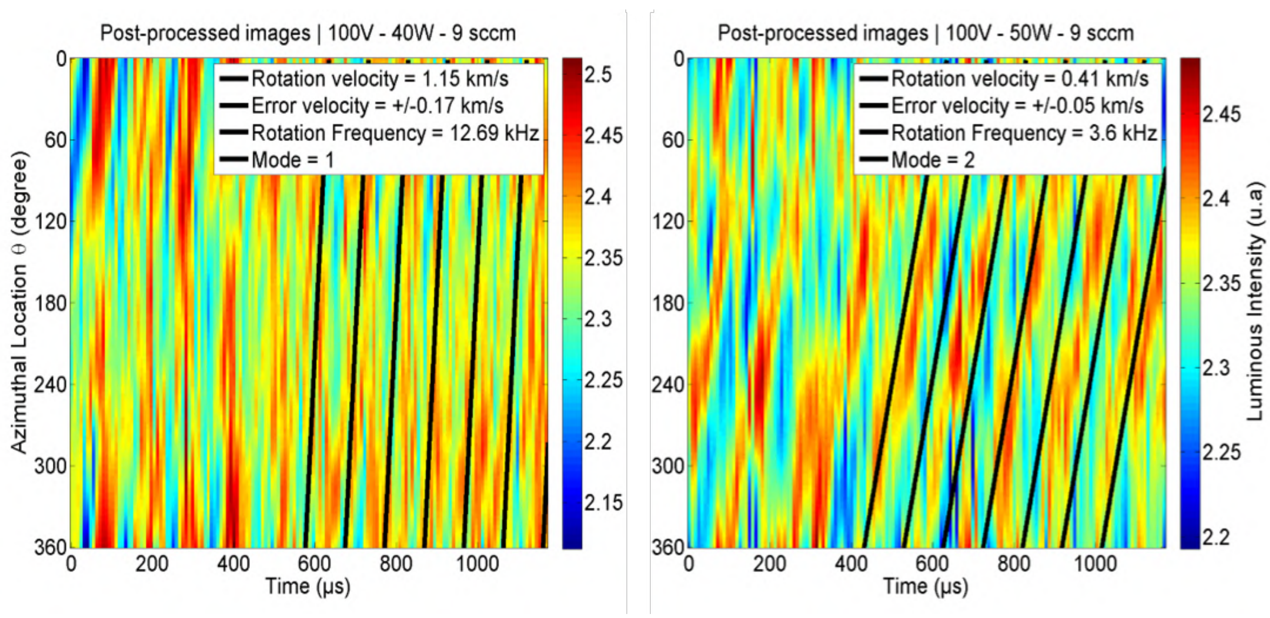

Figure 9. (c) Post-processed images of $L_S(\theta, t)$ for P_{RF} = 40 W and P_{RF} = 50 Wo f RF power injected. The anode mass flow rate is 9 sccm and the discharge voltage is 100V.

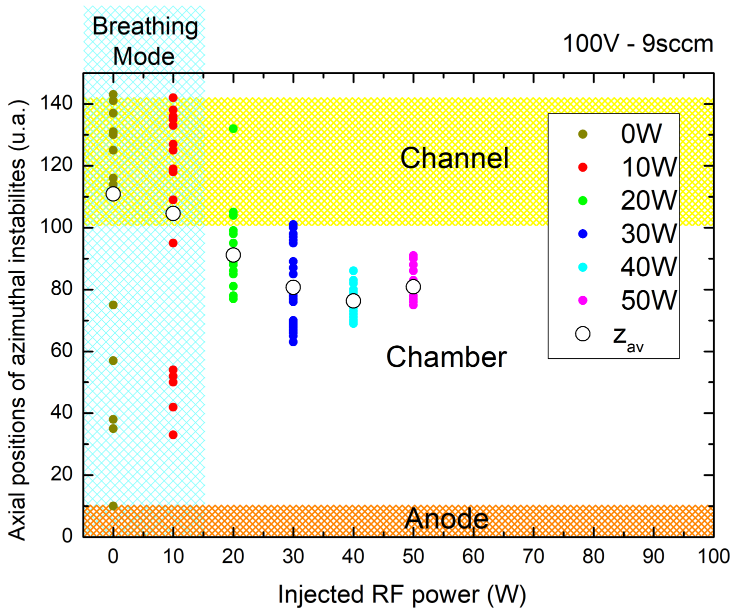

Figure 10. Axial positions of azimuthal instabilities for a discharge voltage of 100 V and for different values of the RF power. The breathing mode is present below 20 W. The xenon mass flow rate is 9 sccm. The white dots circled in black are the average axial positions of the instabilities (the average position is weighted by the size and the light intensity of the spokes).

As described above, using front and side views of the CCD allows to deduce the axial positions of the spokes. Figure 10 shows the axial positions of the instabilities for a discharge voltage of 100 V, and for different values of the injected RF power P_{RF}, from 0W to 50W. The different points for the same RF power in Figure 10 correspond to a measurements of the axial positions of the spokes at different times for 25 to 35 consecutives images. For 0W and 10W, the azimuthal instabilities are distributed from the channel to the anode although the larger and most apparent spokes are located in the channel. Above 10W the azimuthal instabilities are mainly located in the ionization chamber. We measured the axial locations of the spokes as a function of time in the breathing mode and their correlation with the overall light emission intensity. The axial spoke positions are plotted in Figure 11 together with the time variations of the average light intensity of the channel in the breathing oscillations mode for a discharge voltage of 100 V and no RF power in the ionization stage (single stage operation). The size of the spokes is also indicated on the figure. There is a clear correlation between the axial position of the instability and the luminous intensity of the plasma.

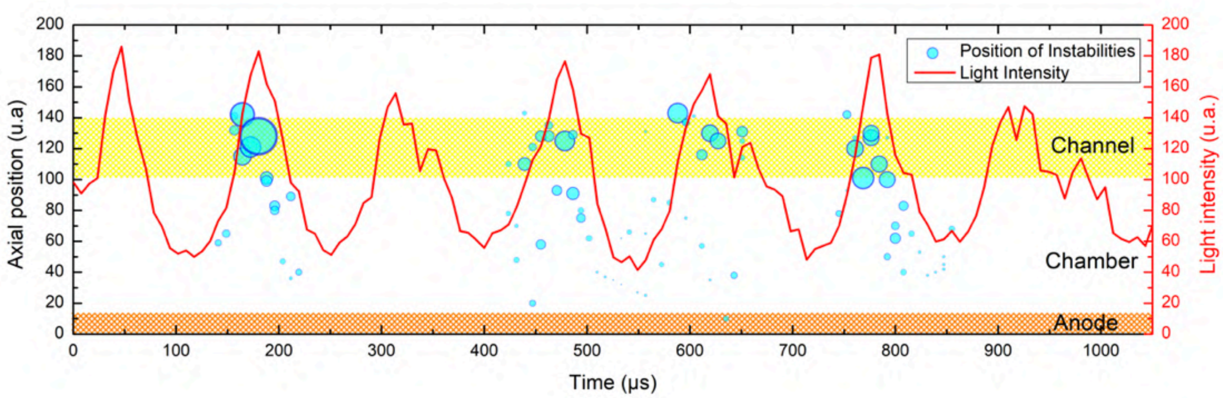

Figure 11 . Positions of axial instabilities (blue circles) as a function of time. The size of the blue circles is proportional to the spoke size. In red is represented the overall light intensity of the channel as a function of time.

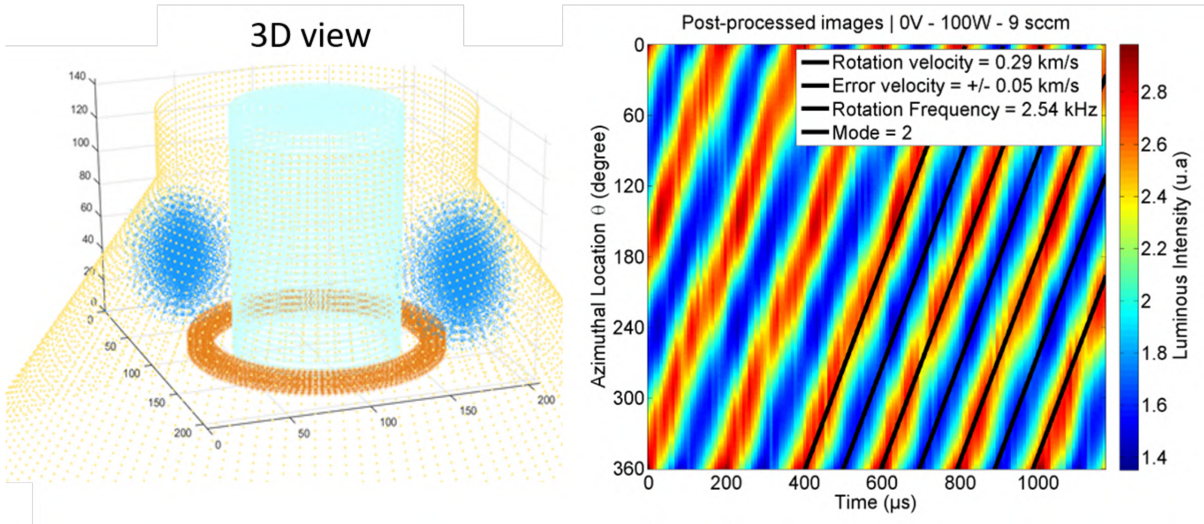

Figure 12. (a) 3D reconstruction of instabilities for one image; (b) Post-processed image of the light intensity of the channel as a function of θ and time in false color representation. Condition: 0V - 100W - 9sccm. Note that the sign of the spoke speed, defined by the slope of the bands observed in the $L_S(\theta, t)$ contours, is opposite to the sign of the slope in the examples of Figure 4 (spoke rotation in the channel). The rotation in the ionization chamber is counterclockwise while the rotation in the channel is clockwise (for a frontal view of the thruster).

Assuming that the time evolution of the light emission of the plasma is in phase with the discharge current, Figure 11 suggests that the main spoke or instability is located in the channel during the rise of the current while smaller and less intense instabilities are present and can be seen in the ionization stage during the decay of the current.

Above 10W of injected RF power, the breathing mode is greatly reduced, the spokes are less visible and move towards the bottom of the channel to ultimately locate in the ionization chamber (Figure 10). In this regime the spokes appear more and more clearly, in a m=2 mode, as the RF power is increased. The plasma rotation in the ionization chamber is especially clear in the case with a zero discharge voltage (only the ionization stage in operation) shown in Figure 12. We observe similar features for a discharge voltage of 100 V and for RF powers from 20 to 50 W (but the images become noisier). This suggests that the spokes observed in this regime of small current fluctuations (no breathing oscillations) are specific to the RF source. Figure 12a displays a 3D reconstruction of the instability and Figure 12b shows the corresponding time variation of the light intensity $L_S(\theta, t)$ for the 0 V-100 W, 9 sccm case. In these conditions, we observe 2 spokes rotating at 290 m/s. These 2 spokes do not seem to be located near the central cylinder, where the magnetic field is small, but in the region of stronger magnetic field, where magnetic field lines tend to be parallel to the conical wall of the ionization stage. The direction of rotation of these spokes is counterclockwise in a frontal view. As said in section II.A, the radial magnetic field in the channel is directed from the outer wall to the inner wall (i.e. the $E \times B$ drift in the thruster channel is clockwise oriented in the azimuthal direction in the frontal view of the thruster). Therefore, the magnetic field along the conical wall is in the cathode-anode direction. Assuming that the electron pressure gradient ∇p near the conical wall is directed radially from the conical wall toward the inner wall, the $\nabla p \times B$ near the conical wall is oriented in the counterclockwise azimuthal direction. One possible interpretation of this result is that the rotating spokes in the ionization chamber could be due to a gradient drift instability. More work is needed to understand the underlying physics of this rotation.

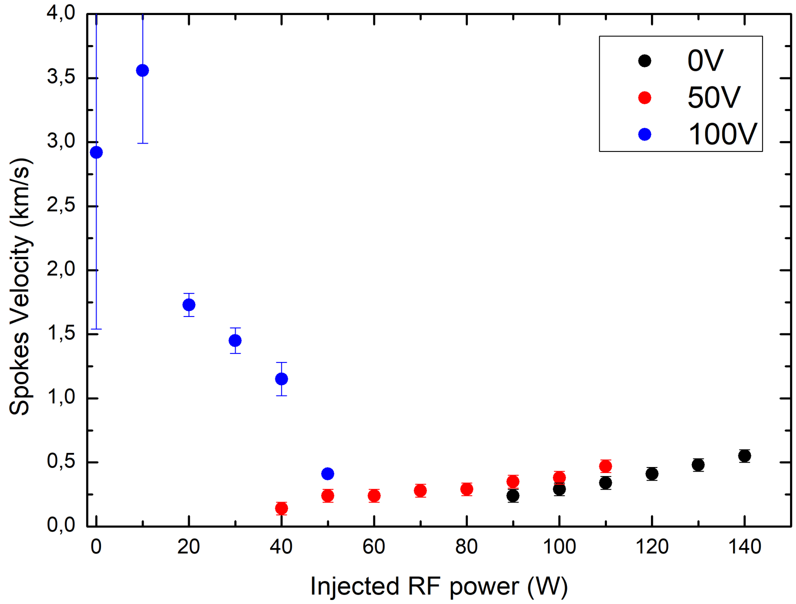

Figure 13. Rotation speed of the spokes as a function of the injected RF power for three values of the discharge voltage (xenon, 9 sccm anode flow rate).

The rotation speed of the spokes, deduced from the front view images, is plotted in Figure 13 as a function of the RF power and for three values of the discharge voltage.

For low values of the discharge voltage, not sufficient to sustain the plasma, i.e. when the plasma generation is mainly due to the ionization stage (0 V, and 50 V cases of Figure 13), we see that the (counterclockwise) rotation speed of the azimuthal instability is small and increases with the RF power (up to about 500s m/s at 100 W RF power). Above 110 W for 50V and 140W for 0V, instabilities are still present but the error bars in the measurements become quite large and we did not plot the corresponding results on Figure 13.

For a discharge voltage of 100 V, sufficient to sustain the discharge in a single stage mode, the speed of the rotating spoke in the channel is much larger, on the order of 2-3 km/s for injected RF powers below 20 W, i.e. in the breathing mode. This (clockwise, i.e. in the $E \times B$ direction) rotation speed is more consistent with previous measurements in single stage thrusters and is close to the acoustic speed of xenon ions for electron temperatures in the 5-10 eV range. Above 10 W RF power for a discharge voltage of 100 V, the rotation speed decreases to smaller values below 500 m/s at 50 W. Above 50 W the rotation speed (not plotted) increases sharply with further increase of the RF power above 50 W but with large uncertainties in the measurements. More generally, the rotation speed increases sharply (with a large decrease of the signal to noise ratio) above an RF power value that decreases with increasing discharge voltage. These trends in the variations of the rotation speed of the spokes with RF power and discharge voltage are still not fully understood.

V.Conclusion

We have performed time-resolved RPA measurements of the Ion Energy Distribution Function and high-speed camera imaging of plasma rotation in the ID-Hall double stage thruster. The results can be summarized as follows:

- Large breathing oscillations of the current are present below a discharge voltage of 190 V in a single-stage regime. The "breathing oscillations mode" disappears above 190 V and the current becomes quasi-constant ("continuous mode", characterized by small amplitude random fluctuations). They also disappear in a double-stage regime if the RF power is above a minimum value that decreases with the discharge voltage (100 W at 190 V[16], 20 W at 100 V).
- In regimes where breathing oscillations are present, the RPA measurements show that the time integrated IEDF presents a relatively wide distribution in energy (sometimes with two distinct peaks). Time-resolved RPA measurements show that the maximum of the IEDF moves in energy during current oscillations. The

time oscillations of the IEDF maximum can be attributed to oscillations of the plasma potential. The plasma potential oscillations are related to the periodic formation of an anodic potential drop (plasma potential below the anode potential) due to the magnetic barrier in front of the anode and to the drop of electron conductivity in front of the anode when the current is minimum. These oscillations disappear for an RF power above the value separating the breathing mode from the continuous mode. The IEDF becomes narrower and steady in this regime.

- CCD imaging with two points of view in front of the thruster, allowing the detection of rotating spokes, their rotation speed and their axial position, has led to the following conclusions:
  - Rotating spokes are present at low voltage in the breathing mode. The most important spokes and instabilities are located in the channel during the current rise but rotating instabilities are also present in the ionization stage during the current decay. The rotation in the channel is in the $E \times B$ direction with a speed on the order of 2-3 km/s, consistent with the acoustic speed of xenon ions for an electron temperature of 5-10 eV.
  - In the continuous mode, i.e. above a given RF power increasing with the discharge voltage, plasma rotation is observed mainly in the ionization stage.
  - This plasma rotation in the ionization stage appears very clearly in the measurements at low discharge voltages. The rotation speed in these conditions is much smaller than the spoke rotation speed in the channel, on the order of a few 100 m/s, increasing with RF power. The spoke rotation in the ionization stage is counterclockwise, i.e. in the $\nabla p \times B$ direction in the region close to the conical wall.

Acknowledgments

This work is supported by CNES, the French Space Agency, and by the RTRA STAE foundation under the project INNPULSE. A. Guglielmi benefits for a PhD fellowship from CNES and Région Occitanie.

References

1. L. Dubois, F. Gaboriau, L. Liard, D. Harribey, C. Henaux, S. Mazouffre, and C. Boniface, in *35th International Electric Propulsion Conference,* IEPC-2017-215, (Atlanta, Ga, 2017).
2. L. Dubois, F. Gaboriau, L. Liard, D. Harribey, C. Henaux, L. Garrigues, G. J. H. Hagelaar, S. Mazouffre, C. Boniface, and J. P. Boeuf, Physics of Plasmas 25 093503 (2018).
3. L. Dubois, F. Gaboriau, L. Liard, C. Boniface, and J. P. Boeuf, Physics of Plasmas 25 093504 (2018).
4. C. Philippe-Kaldec, PhD Thesis, University of Orléans, 1998.
5. M. McDonald and A. D. Gallimore, IEEE Trans. Plasma Sci. 39, 2952 (2011).
6. M. McDonald, C. Bellant, A. S. P. Brandon, and A. Gallimore, in *47th AIAA/ASMA.SAER/ASEE Joint Propulsion Conference,* AIAA 2011-5810, (San Diego, California, 2011).
7. M. MC Donald and J. M. Gallardo, in *32nd International Electric Propulsion Conference,* IEPC-2011-242, (Wiesbaden, Germany, 2011).
8. M. E. Griswold, C. L. Ellison, Y. Raitses, and N. J. Fisch, Phys. Plasmas 19 053506 (2012).
9. C. L. Ellison, Y. Raitses, and N. J. Fisch, Phys. Plasmas 19, 013503 (2012).
10. S. Mazouffre, L. Grimaud, S. Tsikata, K. Matyash, and R. Schneider, Plasma Sources Science and Technology 28, 054002 (2019).
11. M. J. Sekerak, R. R. Hofer, J. E. Polk, B. W. Longmier, A. Gallimore, and D. L. Brown, in *49th AIAA/ASME/SAE/ASEE Joint Propulsion Conference,* AIAA 2013-4116, (San Jose, CA, 2013).
12. M. J. Sekerak, B. W. Longmier, A. D. Gallimore, D. L. Brown, H. R.R., and J. E. Polk, IEEE Trans. Plasma Sci. 43, 72 (2015).
13. M. MC Donald, C. Bellant, B. St. Pierre, and A. D. Gallimore, in *47th AIAA/ASME/SAE/ASEE Joint Propulsion Conference & Exhibit,* AIAA 2011-5810, (San Diego, California, 2011).
14. N. Gascon, M. Dudeck, and S. Barral, Phys. Plasmas 10, 4123 (2003).
15. HALLIS, Software: https://www.hallis-model.com
16. A. Martin Ortega, A. Gugliemi, F. Gaboriau, J. P. Boeuf, and C. Boniface, in *International Electric Propulsion Conference,* IEPC-2019-582, (University of Vienna, Austria, 2019).